HHS Public Access

Author manuscript

Nat Commun. Author manuscript; available in PMC 2015 October 29.

Published in final edited form as:

Nat Commun. ; 6: 7064. doi:10.1038/ncomms8064.

Crystalline silica-induced leukotrieneB_4-dependent inflammation promotes lung tumor growth

Shuchismita R. Satpathy[1,2], **Venkatakrishna R. Jala**[1,2], **Sobha R. Bodduluri**[1,2], **Elangovan Krishnan**[1,2], **Bindu Hegde**[1,2], **Gary Hoyle**[3], **Mostafa Fraig**[4], **Andrew D. Luster**[5], and **Bodduluri Haribabu**[1,2]

[1]James Graham Brown Cancer Center, University of Louisville, Louisville, KY.

[2]Department of Microbiology and Immunology, University of Louisville, Louisville, KY.

[3]Department of Environmental and Occupational Health Sciences, University of Louisville, Louisville, KY.

[4]Department of Pathology & Laboratory Medicine, University of Louisville, Louisville, KY.

[5]Division of Rheumatology, Allergy and Immunology, Center for Immunology and Inflammatory Diseases, Massachusetts General Hospital, Harvard Medical School, Boston, MA.

Abstract

Chronic exposure to crystalline silica (CS) causes silicosis, an irreversible lung inflammatory disease that may eventually lead to lung cancer. In this study, we demonstrate that in K-ras^{LA1} mice, CS exposure markedly enhances the lung tumor burden and genetic deletion of leukotriene B_4 receptor1 (BLT1$^{-/-}$) attenuates this increase. Pulmonary neutrophilic inflammation induced by CS is significantly reduced in BLT1$^{-/-}$K-ras^{LA1} mice. CS exposure induces LTB_4 production by mast cells and macrophages independent of inflammasome activation. In an air pouch model, CS-induced neutrophil recruitment is dependent on LTB_4 production by mast cells and BLT1 expression on neutrophils. In an implantable lung tumor model, CS exposure results in rapid tumor growth and decrease survival that is attenuated in the absence of BLT1. These results suggest that LTB_4/BLT1 axis sets the pace of CS-induced sterile inflammation that promotes lung cancer progression. This knowledge will facilitate development of immunotherapeutic strategies to fight silicosis and lung cancer.

Lung cancer is the single largest cause of cancer-related deaths worldwide. Chronic inflammation considered the seventh hallmark of cancer is promoted by a variety of intrinsic

---

Correspondence to Bodduluri Haribabu, Ph.D. Tel.: 502 852-7503 Fax: 502 852 2123 H0bodd01@louisville.edu.

Author Contributions: SRS and BH conceived of the experiments and wrote the manuscript with comments from ADL. SRS, VRJ, SRB, EK, BH performed experiments and analyzed data. GH assisted in performing surgical instillation of silica and MFC performed histological evaluations. ADL provided reagents and conceptual advice.

The authors declare no competing financial interests.

*Accession Codes

The microarray data have been deposited int eh Gene Expression Omnibus database udner accession code GSE66985.

and extrinsic factors [1-3]. Intrinsic factors such as activating mutation of K-ras, often associated with human lung adenocarcinomas [4] induces a pro-inflammatory microenvironment [5]. Extrinsic factors such as cigarette smoke or air-borne pollutants commonly encountered in the environment, also promote chronic lung inflammation and cancer [6, 7].

Exposure to air-borne particulates such as crystalline silica (CS) is a major global occupational health hazard [8], encountered in diverse array of industrial settings such as mining, pottery, glass and concrete production. Around two million U.S workers and several million more worldwide are occupationally exposed to CS particles. CS exposure leads to lung infiltration of neutrophils, macrophages and lymphocytes causing lung inflammation and the problem is further compounded by massive lung fibrosis leading to the disease silicosis [9, 10]. Silicosis is irreversible and incurable due to impaired particle clearance resulting in persistent lung inflammation and may eventually lead to lung cancer [11, 12]. Epidemiological data suggests that smokers with silicosis are at even higher risk of lung cancer [13, 14]. Though the association of silicosis with lung cancer has been suspected for many decades, there were no established model systems to study mechanisms that link CS-induced chronic inflammation to lung cancer promotion.

Chemokines orchestrate a tightly regulated process of inflammatory cell recruitment to sites of tissue damage, which is a key step in the process of cancer-related inflammation [15, 16]. The lipid chemoattractant LTB_4 is one of the early mediators of inflammation. The high affinity LTB_4 receptor, BLT1 is predominantly expressed on peripheral blood leukocytes and is known to modulate many chronic inflammatory diseases such as arthritis, atherosclerosis, allergic inflammation and insulin resistance during diet-induced obesity [17-20].

In this study, using the K-ras^{LA1} mice that develop spontaneous lung tumors [21], we sought to establish a link between CS-induced chronic inflammation and lung tumor progression. CS exposure led to increased incidence of lung tumors and this process was attenuated in the absence of BLT1. The CS induced pulmonary inflammation and in particular, neutrophil recruitment was abrogated in BLT1$^{-/-}$ mice. Furthermore, CS exposure enhanced the growth of implantable lung tumors leading to reduced survival. Since neutrophils are known to promote lung cancer [22, 23], we investigated the cellular and molecular mechanisms involved in CS-mediated neutrophil recruitment to lungs. The results suggest an intricate interplay of mast cell, macrophage and epithelial cells derived lipid chemoattractant (LTB_4), cytokine (IL-1β) and neutrophil-active chemokines in coordinating CS-induced neutrophil migration. BLT1-mediated recruitment of neutrophils through mast cell produced LTB_4 appears to be the critical initial event in promoting CS-induced inflammation. Collectively, our findings suggest potential for targeting BLT1-mediated neutrophil recruitment for combating silicosis and associated lung cancer.

RESULTS

Absence of BLT1 abrogates the CS-promoted lung tumor growth

Spontaneous activation of K-ras induces an inflammatory microenvironment that promotes tumor growth [24]. To investigate the involvement of BLT1-mediated inflammation in spontaneous K-ras activation-induced lung tumor progression, the BLT1$^{-/-}$K-ras^{LA1} mice were generated. We found that the K-ras^{LA1} mice showed distinctly visible lung tumors at the age of 105 days whereas, the BLT1$^{-/-}$K-ras^{LA1} mice showed fewer and smaller tumors (**Supplementary Fig. 1a)**. Detailed histopathological analysis of lungs performed after serial sectioning of the entire lungs at 200 μm intervals showed that both BLT1$^{+/+}$K-ras^{LA1} and BLT1$^{-/-}$K-ras^{LA1} mice developed similar lung lesions (**Supplementary Fig. 1b)**. However, the numbers of such lesions were significantly reduced in BLT1$^{-/-}$K-ras^{LA1} mice (**Supplementary Fig. 1c**).

To examine the effect of CS exposure on lung tumor growth K-ras^{LA1} mice were instilled with CS. To determine the role of BLT1-mediated inflammation in this process, BLT1$^{-/-}$K-ras^{LA1} mice were also exposed to CS. Equivalent exposure of CS in the lungs of both groups of mice was observed (**Fig. 1a, b**) and tumors were scored in the histological sections. Following CS exposure, the BLT1$^{+/+}$K-ras^{LA1} mice exhibited a significant increase in lung adenomas, the most common histological type found in 100% of each cohort (**Fig. 1 c, d**). In contrast, complete attenuation of increase in lung tumor incidence was observed in CS exposed BLT1$^{-/-}$K-ras^{LA1} mice. These data suggests that CS exposure accelerates lung tumor growth through a process that requires BLT1.

BLT1 controls CS-induced pulmonary neutrophil recruitment

We speculated that CS-mediated increase in lung tumor incidence may be related to increased inflammation, an essential feature of silicosis. A close association of chronic inflammation and tumor promotion has been observed in various types of cancers [1, 25]. Therefore, we investigated the role of BLT1 in regulating CS-mediated chronic inflammation and thus controlling the pace of tumor growth. Histopathological examination of lung sections was carried out to assess inflammation. Features of acute silicosis including neutrophil aggregates, organizing pneumonia, type II pneumocyte proliferation, edema and fibroblastic proliferation as well as chronic inflammation features such as lymphocytic aggregates, expansion of inter-alveolar septa were all observed at 60 days post CS exposure in BLT1$^{+/+}$K-ras^{LA1} mice (**Fig 2a**). Although CS exposed BLT1$^{-/-}$K-ras^{LA1} mice lungs also showed these histological features, the overall inflammation was significantly reduced in these mice (**Fig. 2a, b**). In independent cohorts of CS-treated BLT1$^{+/+}$K-ras^{LA1} mice, analysis of bronchoalveolar lavage fluids (BALF) 60 days post CS exposure by flow cytometry showed a significant increase in different leukocyte populations including neutrophils, macrophages and lymphocytes (**Fig 2c**). Similar increases in macrophages and lymphocytes were also seen in CS exposed BLT1$^{-/-}$K-ras^{LA1} mice but the neutrophil numbers were significantly lower compared to CS exposed BLT1$^{+/+}$K-ras^{LA1} mice (**Fig 2c**). Immunohistochemical analysis also showed similar levels of macrophage infiltration into lungs of both BLT1$^{+/+}$K-ras^{LA1} and BLT1$^{-/-}$K-ras^{LA1} mice (**Supplementary Fig 2**).

Since activated K-ras mutations are known to activate an intrinsic pathway of inflammation, we also analyzed CS-induced inflammation in $BLT1^{+/+}$ and $BLT1^{-/-}$ mice. Significant influx of leukocytes into the airways was observed in these mice (**Fig. 3 a, c**). In airways, neutrophil influx peaked very early at day 2, decreased by day 6 and again increased by day 30. However, neutrophil influx was significantly attenuated during the acute phase at day 2 and the chronic phase at day 30 in $BLT1^{-/-}$ mice (**Fig. 3b, c**). In contrast, macrophage and lymphocyte influx was found to be similar in both $BLT1^{+/+}$ and $BLT1^{-/-}$ mice at 2, 6 or 30 days post CS exposure. To determine whether cellular distribution in the airways reflected changes in the total lungs, whole lung digests were analyzed by flow cytometry. At 2 days post CS exposure there was an increase in neutrophil influx in $BLT1^{+/+}$ mice that was significantly reduced in $BLT1^{-/-}$ mice (**Fig. 3d**).

Absence of BLT1 does not impair CS-induced chemokine production

Since absence of BLT1 was found to attenuate neutrophil recruitment to lungs, we sought to analyze if deletion of BLT1 had an effect on the production of cytokines and chemokines involved in CS-induced neutrophilic inflammation. Levels of the BLT1 ligand LTB_4 were found to significantly increase in BAL fluids of $BLT1^{+/+}$ mice at 2, 6 or 30 days post CS exposure (**Fig. 4a)**. A significant increase in LTB_4 was also observed in $BLT1^{+/+}$K-ras^{LA1} mice (**Fig. 4b)** 60 days post CS exposure. In $BLT1^{-/-}$ mice similar increase in LTB_4 levels was observed at all tested time points, with the exception of day 2 (**Fig 4a and b**).

To determine global changes in CS-induced gene expression profiles total RNA isolated from lungs was analyzed by microarrays. The data analysis indicated that several markers and mediators of inflammation increased in $BLT1^{+/+}$ and $BLT1^{-/-}$ mice at 2 days post CS exposure as well as in $BLT1^{+/+}$K-ras^{LA1} and $BLT1^{-/-}$K-ras^{LA1} mice at 60 days post CS exposure. Of interest, inflammatory cytokines like IL-1β and TNF-α as well as number of chemokines and their receptors were upregulated upon CS exposure (**Supplementary Fig 3**). Real-time PCR analysis confirmed the CS-induced increase in neutrophil-active cytokines and chemokines both at early (day2) and late (day 60) times both in the presence and absence of BLT1 (**Fig 4c and d**). Multiplex analysis of neutrophil active chemokines in BAL fluids also showed significant increase upon CS exposure both in the presence and absence of BLT1 (**Supplementary Fig 4)**. This suggests that neutrophil-active cytokines and chemokines may be produced in the absence of BLT1 signaling and yet are not sufficient to overcome attenuation of neutrophil influx in $BLT1^{-/-}$ lungs.

Cellular mediators of CS-induced inflammation

In inflamed lungs neutrophil-active cytokines and chemokines may be produced from lung resident cells or recruited leukocytes. We next analyzed the CS-induced production of LTB_4, IL-1β and neutrophil-active chemokines *in vitro* by the lung adenocarcinoma cell line derived from K-ras^{LA1} mice-LKR13 [24] and various murine primary cells including macrophages, neutrophils, mast cells and splenocytes. Among the primary cells macrophages and neutrophils but not splenocytes produced LTB_4 upon CS exposure (**Fig 5a**). Bone-marrow derived mast cells produced the highest levels of CS-induced LTB_4 in a dose-dependent manner that peaked by 3 hours (**Fig 5a** and **supplementary Fig. 5a, b**). CS activated murine macrophages produced IL-1β, whereas mast cells and splenocytes did not

secrete IL-1β (**Fig. 5b)**. Primary macrophages and mast cells isolated from murine lungs were also tested for their ability to produce LTB_4 and IL-1β. CS activation of alveolar macrophages led to production of both LTB_4 and IL-1β whereas, lung mast cells produced LTB_4 but not IL-1β post CS exposure (**Fig. 5c, d)**.

The LTB_4 production by CS activation in the macrophage cell-line RAW264.7 was completely blocked by 5-lipoxygenase (5-LO) inhibitor, Zileuton (**Supplementary Fig. 6 a-c)**. The CS-induced LTB_4 was biologically active as determined by chemotaxis of 300.19 cells expressing BLT1 as well as $BLT1^{+/+}$ neutrophils but not the parental 300.19 cells or $BLT1^{-/-}$ neutrophils (**Supplementary Fig. 6d, e**).

Independent regulation of CS-induced LTB_4 and IL1-β production

Since both LTB_4 and IL-1β appear to be critical for silicosis, the inter-dependence of their production was analyzed. CS exposed mast cells from inflammasome pathway-deficient ($NALP3^{-/-}$, $ASC^{-/-}$, $IL\text{-}1\alpha\beta^{-/-}$) or IL-1 response deficient ($IL\text{-}1R^{-/-}$, $MyD88^{-/-}$) as well as $BLT1^{-/-}$ mice secreted LTB_4, but not the $5\text{-}LO^{-/-}$ mast cells (**Fig. 6a)**. As expected, CS treated macrophages from inflammasome pathway-deficient ($NALP3^{-/-}$, $ASC^{-/-}$, $IL\text{-}1\alpha\beta^{-/-}$) mice did not secrete IL-1β, while macrophages from 5-LO pathway deficient ($BLT1^{-/-}$ or $5\text{-}LO^{-/-}$) mice were found to secrete IL-1β similar to wild-type macrophages (**Fig. 6b)**. These data suggest that CS-induced activation of 5-LO and the inflammasome pathway are completely independent of each other and absence of BLT1 does not affect either of the pathways.

Although LKR13 cells did not secrete LTB_4 or IL-1β (**Fig 5a and b**), they produced neutrophil-active chemokines CXCL1, CXCL2, CXCL3, CXCL5 and CCL5 in response to CS stimulation, suggesting that pathways leading to the production of these chemokines are most likely independent of 5-LO or inflammasome activation (**Supplementary Fig. 7**). Many of these chemokines were also produced by both $BLT1^{+/+}$ and $BLT1^{-/-}$ macrophages and mast cells (**Supplementary Fig. 7**).

CS-induced inflammation in an air pouch model requires LTB_4/BLT1 axis—The *in vitro* studies showed that mast cells are a major source of LTB_4 production and the absence of BLT1 clearly reduced lung inflammation and neutrophil influx *in vivo*. Previous studies have shown that CS mediated lung inflammation is dependent on the presence of mast cells [26]. We adopted the murine air-pouch model [27] to assess the contribution of mast cells and the role of LTB_4-BLT1 axis in neutrophil recruitment during CS-induced inflammation. In this model, CS exposure of $BLT1^{+/+}$ mice induced the production of LTB_4 (**Fig 7a**) accompanied by influx of neutrophils (**Fig 7b, c**). This response however was significantly dampened in the $BLT1^{-/-}$ as well as in mast cell deficient mice (**Fig 7a-c**). These data shows that neutrophil recruitment is an early event during CS exposure and is controlled by mast cell-mediated LTB_4 production and expression of BLT1 on neutrophils.

CS-induced inflammation promotes growth of implanted lung tumors

To determine if CS accelerates the growth of implanted lung tumors, we adopted LKR13 s.c. tumor model. LKR-13 cells mixed with CS-particles in matrigel were implanted

subcutaneously into $Rag2^{-/-}$ mice. In $BLT1^{+/+}Rag2^{-/-}$ mice, CS exposure led to a significant increase in tumor growth and consequently reduced their survival (**Fig 8a-d**). Interestingly, the $BLT1^{-/-}Rag2^{-/-}$ mice displayed reduced tumor growth and survival advantage (**Fig 8a-d**). Analysis of immune cell infiltration in these tumors showed that presence of CS resulted in increased neutrophil influx whereas macrophages and mast cells remained unchanged in $BLT1^{+/+}Rag2^{-/-}$ mice (**Fig 8e**). In tumors growing in $BLT1^{-/-}Rag2^{-/-}$ mice neutrophil influx was significantly reduced compared to $BLT1^{+/+}Rag2^{-/-}$ mice whereas the macrophage and mast cell numbers were unchanged. Analysis of neutrophil-active chemokines indicated significant attenuation in the levels of LTB_4, CXCL1and CCL3 in $BLT1^{-/-}$ mice post CS exposure (**Fig 8e, f**). These results emphasize a direct role for CS in promoting lung tumor growth that is dependent on LTB_4/BLT1-mediated inflammation.

DISCUSSION

Exposure to CS has long been associated with increased susceptibility to lung cancer in humans [8]. The results presented here show that CS promotes tumor progression in well-defined spontaneous and implantable mouse lung tumor models. The data suggests that complex interplay of cellular and molecular mediators orchestrate CS-mediated lung inflammation. Mast cells and macrophages produce LTB_4 and IL-1β upon CS exposure leading to sustained neutrophilic inflammation that is further maintained by the chemokines produced by the lung epithelial cells (**Fig 9**). This chronic inflammatory micro-environment promotes lung tumor progression.

Lung tumor progression is associated with activation of both intrinsic and extrinsic pathways of inflammation [1, 2, 7]. Transforming mutations in the K-ras oncogene found in ~30% of human lung adenocarcinomas activate the intrinsic pathway of inflammation by activating NF-kB and consequent production of cytokines and chemokines [28]. Inflammation initiated by extrinsic factors such as exposure to CS may also promote cigarette smoke carcinogen induced tumor progression [8]. While CS has been designated as a human carcinogen by IARC (International Agency for Research on Cancer) [8], the causal relationship of CS exposure and lung cancer progression remained unclear due to lack of experimental model systems. Recent studies have shown that NNK-initiated lung tumor incidence is increased upon CS exposure [29]. In this study, we provide evidence that CS exposure accelerates lung tumor growth in a spontaneous $K\text{-}ras^{LA1}$ mouse model (**Fig 1**) and this enhancement is dependent on BLT1-mediated chronic inflammation (**Fig 2**). Furthermore, the s.c implantable lung tumor model provided direct evidence for the tumor promoting effects of CS (**Fig 8**). Co-implantation of K-ras mutated lung tumor cells with CS resulted in accelerated tumor growth that reduced the survival of tumor bearing mice. In this model also absence of BLT1 reduced the tumor burden and improved survival, suggesting that BLT1 mediated inflammation is a crucial component in CS-induced tumor promotion.

CS exposure is known to induce cell death [30] leading to the recruitment and activation of a variety of leukocytes including mast cells, macrophages and neutrophils. The data herein outlines the cellular and molecular basis for CS-induced inflammation **(Fig. 9)**. Mast cells are known to be essential for the full development of CS-induced lung inflammation and

silicosis [31]. Studies presented here with cultured mast cells showed that CS exposure leads to significantly more LTB_4 production by mast cells relative to other myeloid cells suggesting that mast cell activation is likely an important step in CS-induced inflammation (**Fig 5**). This was further substantiated by the observation of attenuated LTB_4 levels and neutrophils in the CS-exposed air pouch of mast cell deficient mice (**Fig 7**). Mast cell produced LTB_4 along with macrophage secreted LTB_4 and IL-1β, coordinate with the epithelial cell generated chemokines to orchestrate neutrophil migration into inflamed lungs. Although CS exposure also leads to lymphocytic infiltration into lungs, it is known that innate immune processes are sufficient to drive silicosis in the absence of lymphocytes [32]. Consistent with this finding, splenocytes did not produce LTB_4 or IL-1β in response to CS activation (**Fig 5a and b**).

Earlier studies have shown that various cytokines and chemokines such as IL-β, TNF-α, TGF- β, IL-6, IL-8, IL-17A, CCL2 and CCL3 mediate silicosis [33-37]. Among these mediators, production of IL-1β through inflammasome activation appears to be most critical for CS-induced lung inflammation [36, 38-40]. Our study shows that production of LTB_4 is also critical for CS-induced lung inflammation (**Fig 4a, b**). However, in CS exposed lungs absence of BLT1 did not influence production of mediators including IL-1β at early or late times in presence or absence of an activating K-ras mutation *in vivo* (**Fig 4**). Similarly, BLT1 deficiency also did not impact the production of IL-1β or neutrophil-active chemokines by CS exposed cells *in vitro* (**Fig 6b and Supplementary Fig 7**). Moreover, CS-exposure of the inflammasome pathway deficient or IL-1 deficient mast cells did not impact the LTB_4 production (**Fig 6a**). Thus, CS activates parallel pathways for the production of IL-1β and LTB_4. Although neutrophil recruitment was significantly compromised in the absence of BLT1, it was not completely attenuated (**Fig 2c, 3c, 7c and 8c**) possibly due to the production of IL-1β and CC/CXC neutrophil chemokines.

In various inflammatory diseases, relay of molecules that orchestrate recruitment of different cell types are of critical importance towards disease manifestation. In this regard, extremely coordinated tissue chemotaxis of neutrophils in mouse models of inflammatory arthritis [20] or sterile injury [41] were also shown to be initiated by LTB_4. In arthritis models LTB_4/BLT1 axis was critical for initial neutrophil recruitment into the joint leading to the sequential production of IL-1β and neutrophil active chemokine production that sustains joint inflammation. In contrast to these observations, current data shows that absence of BLT1 did not impair production of neutrophil-active cytokine and chemokines in the CS exposed lungs. A reduction in LTB_4 levels observed in air pouch of $BLT1^{-/-}$ mice were possibly due to impairment in recruitment of LTB_4 producing neutrophils (**Fig 7a**). Together, these data suggests that CS exposed mast cells, macrophages and epithelial cells secrete lipids (LTB_4)-cytokines (IL-1β)-chemokines (CXCL, CCL) independently of each other that co-ordinate recruitment of neutrophils. However, LTB_4-BLT1 axis plays the most critical role such that absence of BLT1 significantly dampens this response.

Pro-tumorigenic activity of tumor-associated neutrophils is increasingly being appreciated in lung and other cancers [23, 42-45]. Inhibition of CXCR2-mediated neutrophil infiltration into lung tumors was shown to be associated with reduced tumor growth [23, 28, 46]. Neutrophil numbers within the tumor correlates to poor prognosis in NSCLC [47].

Interestingly, in NSCLC patients an increase of neutrophil chemoattractants LTB_4 and IL-8 in exhaled breath condensate were reported [48]. Again, levels of LTB_4 and IL-8 were found to increase with progression of NSCLC stages I through IV indicating the importance of LTB_4 and IL-8 in recruiting neutrophils into lung tumors. Thus, a common feature of lung cancer progression appears to be association of neutrophils in the tumor. The results presented here show a strong correlation between rapid tumor growth and increased neutrophilic inflammation both in spontaneous and implantable lung tumor models. Furthermore, neutrophil recruitment is dependent on BLT1 expression under different settings including the lungs of $Kras^{LA1}$ mice, skin air pouch and in the s.c. implantable tumor models suggesting a critical function for LTB_4/BLT1 axis in regulating CS-mediated inflammation. While the neutrophilic inflammation is most likely mediator of CS-promoted tumor progression, further studies are required to establish a direct cause and effect relationship in these models.

Methods

Mice

All mice were on C57BL/6 background and were sex and - age matched at 6-7 weeks. K-ras^{LA1} mice was obtained from NCI mouse repository and subsequently crossed onto $BLT1^{-/-}$ background to generate $BLT1^{-/-}$K-ras^{LA1} mice. $Rag2^{-/-}$ mice was obtained from Taconic (Germantown, NY) and subsequently crossed onto $BLT1^{-/-}$ background to generate $BLT1^{-/-}Rag2^{-/-}$ mice. C57BL/6J ($BLT1^{+/+}$), $Kit^{W\text{-}sh/W\text{-}sh}$, $MyD88^{-/-}$ mice were purchased from Jackson Laboratories. $BLT1^{-/-}$ mice were described previously [49]. IL-1$\alpha\beta^{-/-}$ and 5-$LO^{-/-}$ mice were from Dr. A. Luster. IL-$1R^{-/-}$ mice were kindly provided by Dr. Jun Yan at the University of Louisville. Bone marrow from $NALP3^{-/-}$ and $ASC^{-/-}$ mice were provided by Dr. Kate Fitzgerald at the University of Massachusetts. All mice were maintained under specific pathogen-free conditions and all the procedures were approved by University of Louisville Institutional Animal Care and Use Committee.

CS instillation in mouse lungs

Crystalline silica (MIN-U-SIL-5; average particle diameter 1.7μm) was obtained from U.S. Silica Co., WV and was made endotoxin-free by baking at 200°C overnight. 45 days old $BLT1^{+/+}$, $BLT1^{-/-}$, $BLT1^{+/+}$K-ras^{LA1} and $BLT1^{-/-}$K-ras^{LA1} mice were either left untreated or surgically instilled (intra-tracheal) with endotoxin-free PBS (vehicle) or 2mg of endotoxin-free crystalline silica suspended in vehicle without sonication. CS particle suspension was vortexed before instillation to avoid settling of the particles. Mice were treated with antibiotics for a week before surgery and were continuously maintained on antibiotics until euthanized. Lungs from $BLT1^{+/+}$K-ras^{LA1} and $BLT1^{-/-}$K-ras^{LA1} mice were analyzed 60 days after PBS or CS instillation and lungs from $BLT1^{+/+}$, $BLT1^{-/-}$ mice were analyzed after 2, 6 or 30 days after PBS or CS instillation as indicated.

CS-induced inflammation in air pouch model

Six to eight weeks old mice were used to generate air pouch as described previously [50]. Briefly, mice were injected subcutaneously with 5 ml of sterile air into the back to generate the air pouch. After 3 days another 3ml of sterile air was injected into the pouch. 3 days

later, 1mg of CS in 500μl of endotoxin-free PBS was injected into the air pouch. Control animals received only 500μl of endotoxin-free PBS. 6 hours later animals were euthanized and air pouch was lavaged with 3ml of PBS.

CS-promotion of implantable lung tumors

LKR13 cells used in this study were kindly provided by Dr. Tyler Jacks [28]. To establish LKR13 tumors [51], 2×10^6 live LKR13 cells in presence of 2mg CS particles were resuspended in 100 μl PBS, mixed with 100 μl matrigel (Corning) and injected subcutaneously into the right flank of naive six to eight weeks old $BLT1^{+/+}Rag2^{-/-}$ and $BLT1^{-/-}Rag2^{-/-}$ mice. Mice injected subcutaneously with LKR13 cells alone served as controls. Tumor growth was monitored two to three times per week, and tumor size was measured in millimeters using a caliper. Average tumor size was calculated by measuring two perpendicular diameters. Animals bearing tumors were euthanized when tumors reached a size of 15 mm in one of the two perpendicular diameters or earlier if tumors ulcerated or animal showed signs of discomfort.

Lung histopathology

105 days old $BLT1^{+/+}$K-ras^{LA1} and $BLT1^{-/-}$K-ras^{LA1} mice were analyzed for lung tumor burden. Lungs were inflated with 10% buffered formalin and were then removed, fixed in 10% buffered formalin for 24 h and stored in 70% ethanol. Lung lobes were separated and processed, embedded in paraffin and serially sectioned. Mid-sagittal 5 μm serial lung sections (200μm apart) were stained with haematoxylin and eosin and digitally scanned on Aperio ScanScope. Lung sections were analyzed by an experienced pulmonary pathologist. Lung lesions (hyperplasia-H, adenomatous hyperplasia -AH, and adenoma- A) based on the histological features [52] were enumerated on the entire lung section using the digital image. Digital images of lung sections were also used to analyze lung inflammation. Lung inflammation is quantified as the percentage of inflamed lung area to total lung area in H&E stained lung sections. Lung tissue macrophages in the sections were identified by immuno-histochemistry (IHC). Sections were stained with 1:50 diluted Rat anti-mouse F4/80 antibody (clone CL:A3-1, cat.# MCA497G, AbD Serotec) at the Pathology Core Research Laboratory at University of Louisville, following standard protocol. Five independent fields per mouse lung section were randomly selected for macrophage counting and average macrophages per field were represented. Crystalline silica particles in the lungs sections were viewed under polarized light and lungs were semi-quantitatively scored on a scale of 1-3 for the amount of deposited particles.

Immune cell identification by flow cytometry

Leukocytes were collected from airways, air pouch or peritoneal cavity by lavage; from unlavaged whole lungs, LKR13 subcutaneous tumors, spleen or cultures of bone marrow derived macrophages, mast cells. Single cell suspension was obtained from whole lungs or subcutaneous tumors by digesting the tissue in an enzyme mixture consisting of collagenase A (2 mg/ml), DNase I (100 μg/ml) for 1 h at 37°C with occasional vortexing. The digested tissue was filtered through a nylon mesh, and the resultant cells were washed twice in PBS. 2×10^6 cells in single-cell suspensions were incubated with F_C-receptor blocking antibody followed by staining with various cell surface marker antibodies from BD Biosciences (San

Diego, CA) or Biolegend (San Diego, CA), following standard protocols. Flow cytometry data were acquired on FACS Calibur or FACS Canto (BD Biosciences) and analyzed using Flowjo software (Tree Star).

In the lung tissue and airways (BALF), leukocytes were identified as $CD45^+$ cells, alveolar or lung macrophages as $CD45^+$ FSC^{hi} $CD11c^{hi}$ $F4/80^+$ cells, neutrophils as $CD45^+$ $CD11c^-$ $Ly6G^{hi}$ Siglec-F^- cells, B cells as $CD45^+$ FSC^{lo} $B220^+$ cells, CD4 cells as $CD45^+$ FSC^{lo} $CD4^+$ and CD8 cells as $CD45^+$ FSC^{lo} $CD8^+$. In peritoneal cavity, macrophages were identified as $CD45^+$ FSC^{hi} $F4/80^+$ cells and neutrophils as $CD45^+$ SSC^{hi} $Ly6G^{hi}$ cells. In spleen B cells were $CD45^+$ FSC^{lo} $B220^+$ and T cells were $CD45^+$ FSC^{lo} $CD3^+$. Macrophages from bone marrow cultures were $CD11b^+$ $F4/80^+$ and mast cells from bone marrow cultures were $CD117^+$ $Fc\varepsilon R1^+$. In the subcutaneous tumors, leukocytes were identified as $CD45^+$ cells, macrophages as $CD45^+$ FSC^{hi} $F4/80^+$ $CD11b^{hi}$ $Ly6G^{lo}$cells, mast cells as $CD45^+$ $CD117^+$ $Fc\varepsilon R1^+$ and neutrophils as $CD45^+$ SSC^{hi} $Ly6G^{hi}$cells. In air pouch lavage fluid, leukocytes were identified as $CD45^+$ cells, macrophages as $CD45^+$ FSC^{hi} $F4/80^+$ $CD11b^{hi}$ $Ly6G^{lo}$cells and neutrophils as $CD45^+$ SSC^{hi} $Ly6G^{hi}$cells. Cytospin preparations of the air pouch lavage fluid cells were also done using Shandon Cytospin centrifuge (Shandon Lipshaw) followed by staining with Hema-3 reagents (Fisher Scientific) according to the manufacturer's recommendations.

Isolation of lung mast cells and alveolar macrophages

Cells obtained from pooled lung digests of 4 naïve WT (wild-type) mice were treated with RBC lysis buffer (BD Biosciences), resuspended in DMEM containing 10% FBS and incubated at 37°C. The non-adherent cells were transferred after 8 hours into fresh tubes without disturbing the adherent (macrophages and fibroblast) cells. The non-adherent cells were then incubated with F_C-receptor blocking antibody followed by staining for CD45, CD117 and FcεR1 in 5% BSA (Bovine serum albumin). Mast cells identified as FSC^{hi} $CD45^+$ $CD117^+$ $Fc\varepsilon R1^+$ cells were sorted using BD FACS Aria III cell sorter. Purity of the cells was 95.3%.

Whole lung lavage from 10 naïve WT mice were pooled, resuspended in DMEM containing 10% FBS and incubated at 37°C for 4 hours. The non-adherent cells were discarded and alveolar macrophages were obtained by dislodging the adherent cells, followed by staining for CD45 and F4/80 after blocking F_C-receptors. Purity of cells was 99.5%.

Isolation and culture of primary murine cells

Bone marrow-derived mast cells (BMMC) were prepared from 6-8 weeks old mice of indicated genotypes. Briefly, bone marrow cells were flushed out and cultured in DMEM containing 10% FBS,100 units/ml Penicillin, 100 μg/ml Streptomycin, 2 mM L-Glutamine, 50 μM β-mercaptoethanol supplemented with 12.5 ng/ml recombinant Mouse SCF (R&D # 455 MC,10 μg/ml Stock,) and 10 ng /ml recombinant Mouse IL-3 (R&D #403-ML,10 μg/ml Stock). The bone marrow cells were plated at ~1×10^6 /ml density in T-75 cm^2 flask containing 15 ml of medium. The non-adherent cells were transferred after 48 hours into fresh flasks without disturbing the adherent (fibroblast) cells. The flasks were changed weekly or as needed to separate the non-adherent mast cells from the contaminating

adherent cells. The medium was changed once a week with medium containing SCF, IL-3. The homogenous population of mast cells was visible after 4 weeks of culture and propagated further for 4 weeks. The purity of BMMCs derived from WT or various KO (knock out) mice was confirmed to be ≥99% by surface staining for mast cell specific markers CD117 and FcεR1.

Bone marrow derived macrophages (BMDM) were prepared from 6-8 weeks old mice of indicated genotypes. Briefly, bone marrow cells were flushed out and cultured in DMEM containing 10% FBS,100 units/ml Penicillin, 100 μg/ml Streptomycin, 2 mM L-Glutamine, 50 μM β-mercaptoethanol supplemented with 100 ng/ml recombinant Mouse MCSF (Biolegend). The bone marrow cells were plated at 0.6×10^6 /ml density in 100mm tissue culture dishes containing 10 ml of medium. After 3 days medium was replaced by 10ml of fresh growth medium and a homogenous population of macrophages was visible. The cultures were maintained for another 3 days before stimulation. The cells were found to be more than 99% pure as confirmed by surface staining for F4/80 and CD11b. Eight weeks old mice were injected intraperitoneally with 2ml of 3% aged thioglygollate medium. Peritoneum was lavaged after 10 h or 4 days to obtain elicited neutrophils and macrophages respectively. The purity of thioglycollate elicited neutrophils and macrophages; resident peritoneal macrophages were ≥ 95%.

For CS stimulation assays, mast cells from various sources were plated at 0.3 million per well of 12-well tissue culture dishes in 400μl of medium without FBS. Primary macrophages from various sources, splenocytes and neutrophils were plated at 0.3 million per well of 12-well tissue culture dishes in 400μl of 1% FBS containing medium. All primary cells were stimulated with 100 $\mu g/cm^2$ of CS for 6 h. Primary macrophages from all sources were primed with 10ng/ml of LPS (InvivoGen) for 3 h prior to CS stimulation.

LKR13 and RAW264.7cells were cultured in DMEM containing 10% FBS. For CS stimulation assays, 0.3 million cells were plated per well of 12-well tissue culture dishes in 400μl of 1% FBS containing medium.The cells were stimulated for 6 h with 120 $\mu g/cm^2$ of CS. Whenever indicated RAW264.7 cells were pre-treated with 10 μM Zileuton (5-LO inhibitor) for 1h.

Cell migration assay

Chemotaxis of 300.19 cells and thioglycollate elicited peritoneal neutrophils was evaluated using 5-μm pore size Transwell filters (Corning Costar, Cambridge, MA). Briefly, 1 million cells in 100 μl of medium were loaded onto the upper chamber. The lower chamber was loaded with 600 μl of either medium alone or 0.3nM LTB_4 or unstimulated RAW264.7 cell supernatants or 120$\mu g/cm^2$ of CS stimulated RAW264.7 cell supernatants. After 3 h of incubation at 37°C in 5% CO_2, the upper chamber was removed and cells that migrated to the lower chamber was counted.

LTB_4 and IL-1β quantification

Subcutaneous tumors were homogenized in 500 ul 1x PBS buffer containing 10uM Indomethacin using Omni GLH general homogenizer. The homogenates were centrifuged at 14000 g for 10 min and LTB_4 levels in the supernatants were quantified. The LTB_4 levels

were normalized to the amount of protein in the supernatants measured by Themo Sceintific Pierce BCA protein assay kit following manufacturer's instructions. LTB_4 in the tumor homogenate supernatant was expressed as pg/mg of protein. LTB_4 in cell culture supernatants, BALF, air pouch lavage and subcutaneous tumors was measured using LTB_4 EIA Kit (Cayman Chemical) according to the manufacturer's instructions. IL-1β in cell culture supernatants was measured using Mouse IL-1β ELISA MAX™ Standard Kit (Biolegend) according to the manufacturer's instructions.

Quantitative RT-PCR

Total RNA from LKR13 cells, bone marrow-derived macrophages and mast cells, subcutaneous tumors as well as lungs was isolated using an RNeasy Mini Kit (Qiagen) in accordance with the manufacturer's protocol. RNA samples were treated with DNase (Qiagen) before reverse transcription with TaqMan reverse transcription reagents (Applied Biosystems) using random hexamer primers. Quantitative PCR analyses were conducted as described previously[53] using 'power SYBR-green master mix' (Applied Biosystems). Expression of the target genes was normalized to *GAPDH* and the relative fold changes were calculated using the delta CT method. The fold changes were displayed relative to the PBS (vehicle) treated $BLT1^{+/+}$ samples or LKR13 injected $BLT1^{+/+}Rag2^{-/-}$ group. Data were representative of tissues isolated from at least 5 different mice for each cohort or triplicate cell cultures. The GAPDH, IL-1β, TNF-α, CXCL1, CXCL2, CXCL3, CXCL5, CCL2, CCL3, CCL4, CCL5, CXCR1, CXCR2 and *CCR5* primers obtained from RealTimePrimers.com were used in this study.

Microarray and data analysis

Total RNA was prepared from mouse lung tissues as described above. The micro array was performed using Affymetrix GeneChip®Mouse Gene 1.0 ST Array according to manufacturer's protocol at the University of Louisville genomics facility. . The GeneChip-brand array comprised of over 750,000 unique 25-mer oligonucleotide features constituting over 28,000 gene level probes with an average of 27 probes per gene. Briefly, Total RNA was amplified and labeled following the Affymetrix (Santa Clara, CA) standard protocol for whole transcript expression analysis, followed by hybridization to Affymetrix Mouse Gene 1.0 ST® arrays. The arrays were processed following the manufacturer recommended wash and stain protocol on an Affymetrix FS-450 fluidics station and scanned on an Affymetrix GeneChip® 7G scanner using Command Console 3.1 . The resulting .cel files were imported into Partek Genomics Suite 6.6 and transcripts were normalized on a gene level using RMA as normalization and background correction method. Contrasts in a 1-way ANOVA were set up to compare the treatment groups of interest. The fold changes in gene expression along with Affymetrix IDs, p-values were uploaded on to MetaCore pathway analysis software. The fold change in cytokines, chemokines and their receptors were displayed relative to the PBS (vehicle) treated $BLT1^{+/+}$ sample and represented in graphs. Data were representative of pooled lung tissue RNA isolated from 3 different mice for each group. The data from the array analysis has been deposited in the NCBI public access database (http://www.ncbi.nlm.nih.gov/geo/query/acc.cgi?acc=GSE66985).

Multiplex analysis

Whole lung lavage fluids from PBS or CS treated BLT1$^{+/+}$K-ras^{LA1} and BLT1$^{-/-}$K-ras^{LA1} or BLT1$^{+/+}$ and BLT1$^{-/-}$ mice were analyzed for levels of various inflammatory proteins namely TNF-α, CXCL1, CCL3, CCL4 and CCL5. The analysis was performed following standard protocols at the Proteomics core facility of Medical University of South Carolina.

Data analysis

All data are analyzed with GraphPad Prism4 Software, San Diego, CA and expressed as the means ± s.e from at least three independent samples. Statistical difference among groups was analyzed using the Mann–Whitney *U*-test (*in vivo*) or Unpaired Student's t-test (*in vitro/ex-vivo*, RNA analysis). Two-tailed *P* values of <0.05 were considered as significant.

Supplementary Material

Refer to Web version on PubMed Central for supplementary material.

Acknowledgements

We thank Dr. Jason Chesney for critical reading of the manuscript. This work was supported by the NIH grant R01CA138623, NIH: 1P30GM106396-01 (UofL J. G. Brown Cancer Center Phase III CoBRE) and by research grants from Kentucky Lung Cancer Research Board as well as Institutional support from the James Graham Brown Cancer Center. Dr. Satpathy is supported by a postdoctoral award from the James Graham Brown foundation.

REFERENCES

1. Mantovani A, et al. Cancer-related inflammation. Nature. 2008; 454(7203):436–44. [PubMed: 18650914]
2. Houghton AM. Mechanistic links between COPD and lung cancer. Nat Rev Cancer. 2013; 13(4): 233–45. [PubMed: 23467302]
3. Colotta F, et al. Cancer-related inflammation, the seventh hallmark of cancer: links to genetic instability. Carcinogenesis. 2009; 30(7):1073–81. [PubMed: 19468060]
4. Russo M, Di Nicolantonio F, Bardelli A. Climbing RAS, the everest of oncogenes. Cancer Discov. 2014; 4(1):19–21. [PubMed: 24402942]
5. Ji H, et al. K-ras activation generates an inflammatory response in lung tumors. Oncogene. 2006; 25(14):2105–12. [PubMed: 16288213]
6. Elinav E, et al. Inflammation-induced cancer: crosstalk between tumours, immune cells and microorganisms. Nat Rev Cancer. 2013; 13(11):759–71. [PubMed: 24154716]
7. Takahashi H, et al. Tobacco smoke promotes lung tumorigenesis by triggering IKKbeta- and JNK1-dependent inflammation. Cancer Cell. 2010; 17(1):89–97. [PubMed: 20129250]
8. Leung CC, Yu IT, Chen W. Silicosis. Lancet. 2012; 379(9830):2008–18. [PubMed: 22534002]
9. Huaux F. New developments in the understanding of immunology in silicosis. Current opinion in allergy and clinical immunology. 2007; 7(2):168–73. [PubMed: 17351471]
10. Takato H, et al. The specific chymase inhibitor TY-51469 suppresses the accumulation of neutrophils in the lung and reduces silica-induced pulmonary fibrosis in mice. Exp Lung Res. 2011; 37(2):101–8. [PubMed: 21128860]
11. Brown T. Silica exposure, smoking, silicosis and lung cancer--complex interactions. Occup Med (Lond). 2009; 59(2):89–95. [PubMed: 19233828]
12. Cox LA Jr. An exposure-response threshold for lung diseases and lung cancer caused by crystalline silica. Risk Anal. 2011; 31(10):1543–60. [PubMed: 21477084]

13. Liu Y, et al. Exposure-response analysis and risk assessment for lung cancer in relationship to silica exposure: a 44-year cohort study of 34,018 workers. Am J Epidemiol. 2013; 178(9):1424–33. [PubMed: 24043436]
14. Kachuri L, et al. Occupational exposure to crystalline silica and the risk of lung cancer in Canadian men. Int J Cancer. 2013
15. Balkwill F. Cancer and the chemokine network. Nat Rev Cancer. 2004; 4(7):540–50. [PubMed: 15229479]
16. Ruffini PA, et al. Manipulating the chemokine-chemokine receptor network to treat cancer. Cancer. 2007; 109(12):2392–404. [PubMed: 17503430]
17. Oyoshi MK, et al. Leukotriene B4-driven neutrophil recruitment to the skin is essential for allergic skin inflammation. Immunity. 2012; 37(4):747–58. [PubMed: 23063331]
18. Li RC, et al. Leukotriene B4 Receptor-1 Mediates Intermittent Hypoxia-induced Atherogenesis. American journal of respiratory and critical care medicine. 2011; 184(1):124–31. [PubMed: 21493735]
19. Spite M, et al. Deficiency of the Leukotriene B4 Receptor, BLT-1, Protects against Systemic Insulin Resistance in Diet-Induced Obesity. Journal of immunology. 2011
20. Chou RC, et al. Lipid-cytokine-chemokine cascade drives neutrophil recruitment in a murine model of inflammatory arthritis. Immunity. 2010; 33(2):266–78. [PubMed: 20727790]
21. Johnson L, et al. Somatic activation of the K-ras oncogene causes early onset lung cancer in mice. Nature. 2001; 410(6832):1111–6. [PubMed: 11323676]
22. Houghton AM, et al. Neutrophil elastase-mediated degradation of IRS-1 accelerates lung tumor growth. Nature medicine. 2010; 16(2):219–23.
23. Gong L, et al. Promoting effect of neutrophils on lung tumorigenesis is mediated by CXCR2 and neutrophil elastase. Mol Cancer. 2013; 12(1):154. [PubMed: 24321240]
24. Wislez M, et al. High expression of ligands for chemokine receptor CXCR2 in alveolar epithelial neoplasia induced by oncogenic kras. Cancer Res. 2006; 66(8):4198–207. [PubMed: 16618742]
25. Grivennikov SI, Greten FR, Karin M. Immunity, inflammation, and cancer. Cell. 2010; 140(6): 883–99. [PubMed: 20303878]
26. Brown JM, et al. Silica-directed mast cell activation is enhanced by scavenger receptors. Am J Respir Cell Mol Biol. 2007; 36(1):43–52. [PubMed: 16902192]
27. Colville-Nash P, Lawrence T. Air-pouch models of inflammation and modifications for the study of granuloma-mediated cartilage degradation. Methods Mol Biol. 2003; 225:181–9. [PubMed: 12769487]
28. Wislez M, et al. High expression of ligands for chemokine receptor CXCR2 in alveolar epithelial neoplasia induced by oncogenic kras. Cancer research. 2006; 66(8):4198–207. [PubMed: 16618742]
29. Bode C, et al. Suppressive oligodeoxynucleotides reduce lung cancer susceptibility in mice with silicosis. Carcinogenesis. 2014; 35(5):1078–83. [PubMed: 24403310]
30. Hamilton RF Jr. Thakur SA, Holian A. Silica binding and toxicity in alveolar macrophages. Free Radic Biol Med. 2008; 44(7):1246–58. [PubMed: 18226603]
31. Suzuki N, et al. Mast cells are essential for the full development of silica-induced pulmonary inflammation: a study with mast cell-deficient mice. Am J Respir Cell Mol Biol. 1993; 9(5):475–83. [PubMed: 8217187]
32. Beamer CA, et al. Innate immune processes are sufficient for driving silicosis in mice. J Leukoc Biol. 2010; 88(3):547–57. [PubMed: 20576854]
33. Piguet PF, et al. Requirement of tumour necrosis factor for development of silica-induced pulmonary fibrosis. Nature. 1990; 344(6263):245–7. [PubMed: 2156165]
34. Yao SQ, et al. Role of Fas/FasL pathway-mediated alveolar macrophages releasing inflammatory cytokines in human silicosis. Biomed Environ Sci. 2013; 26(11):930–3. [PubMed: 24331540]
35. Chen Y, et al. Neutralization of interleukin-17A delays progression of silica-induced lung inflammation and fibrosis in C57BL/6 mice. Toxicol Appl Pharmacol. 2014; 275(1):62–72. [PubMed: 24291675]

36. Cassel SL, et al. The Nalp3 inflammasome is essential for the development of silicosis. Proc Natl Acad Sci U S A. 2008; 105(26):9035–40. [PubMed: 18577586]
37. Wang X, et al. Silencing CD36 gene expression results in the inhibition of latent-TGF-beta1 activation and suppression of silica-induced lung fibrosis in the rat. Respir Res. 2009:36. [PubMed: 19439069]
38. Dostert C, et al. Innate immune activation through Nalp3 inflammasome sensing of asbestos and silica. Science. 2008; 320(5876):674–7. [PubMed: 18403674]
39. Guo J, et al. Neutralization of interleukin-1 beta attenuates silica-induced lung inflammation and fibrosis in C57BL/6 mice. Arch Toxicol. 2013; 87(11):1963–73. [PubMed: 23640035]
40. Hornung V, et al. Silica crystals and aluminum salts activate the NALP3 inflammasome through phagosomal destabilization. Nature immunology. 2008; 9(8):847–56. [PubMed: 18604214]
41. Lammermann T, et al. Neutrophil swarms require LTB4 and integrins at sites of cell death in vivo. Nature. 2013; 498(7454):371–5. [PubMed: 23708969]
42. Fridlender ZG, Albelda SM. Tumor-associated neutrophils: friend or foe? Carcinogenesis. 2012; 33(5):949–55. [PubMed: 22425643]
43. Gregory AD, Houghton AM. Tumor-associated neutrophils: new targets for cancer therapy. Cancer Res. 2011; 71(7):2411–6. [PubMed: 21427354]
44. Mantovani A, et al. Neutrophils in the activation and regulation of innate and adaptive immunity. Nat Rev Immunol. 2011; 11(8):519–31. [PubMed: 21785456]
45. Shang K, et al. Crucial involvement of tumor-associated neutrophils in the regulation of chronic colitis-associated carcinogenesis in mice. PLoS One. 2012; 7(12):e51848. [PubMed: 23272179]
46. Tazzyman S, et al. Inhibition of neutrophil infiltration into A549 lung tumors in vitro and in vivo using a CXCR2-specific antagonist is associated with reduced tumor growth. Int J Cancer. 2011; 129(4):847–58. [PubMed: 21328342]
47. Ilie M, et al. Predictive clinical outcome of the intratumoral CD66b-positive neutrophil-to-CD8-positive T-cell ratio in patients with resectable nonsmall cell lung cancer. Cancer. 2012; 118(6): 1726–37. [PubMed: 21953630]
48. Carpagnano GE, et al. Neutrophilic airways inflammation in lung cancer: the role of exhaled LTB-4 and IL-8. BMC Cancer. 2011; 11:226. [PubMed: 21649887]
49. Haribabu B, et al. Targeted disruption of the leukotriene B(4) receptor in mice reveals its role in inflammation and platelet-activating factor-induced anaphylaxis. J Exp Med. 2000; 192(3):433–8. [PubMed: 10934231]
50. Sin YM, et al. Mast cells in newly formed lining tissue during acute inflammation: a six day air pouch model in the mouse. Ann Rheum Dis. 1986; 45(10):873–7. [PubMed: 3789822]
51. Zhang L, et al. A novel immunocompetent murine model for replicating oncolytic adenoviral therapy. Cancer Gene Ther. 2015; 22(1):17–22. [PubMed: 25525035]
52. Nikitin AY, et al. Classification of proliferative pulmonary lesions of the mouse: recommendations of the mouse models of human cancers consortium. Cancer research. 2004; 64(7):2307–16. [PubMed: 15059877]
53. Mathis SP, et al. Nonredundant roles for leukotriene B4 receptors BLT1 and BLT2 in inflammatory arthritis. J Immunol. 2010; 185(5):3049–56. [PubMed: 20656922]

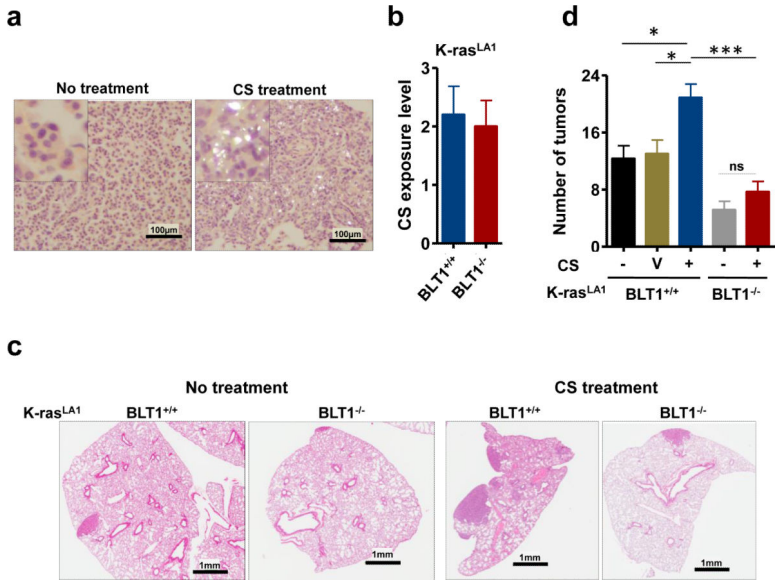

Figure 1. CS-promoted lung tumor progression is abrogated in the absence of BLT1

Forty five days old BLT1$^{+/+}$K-ras^{LA1} and BLT1$^{-/-}$K-ras^{LA1} mice were exposed to CS by intra-tracheal instillation as described in methods. Sixty days post CS instillation; lungs from these mice were analyzed for CS particle deposition and tumor multiplicity. (**a**) Representative lung H&E sections showing deposited CS particles; scale bars, 100μm; insets show CS particles at higher magnification. (**b**) Lung CS exposure was determined based on semi-quantitative scoring (scale of 0-3) of CS particle deposition in sections; n=5 for both groups. (**c**) Representative lung lobe sections showing adenomas; scale bars, 1mm. (**d**) Quantification of adenomas from all serial lung sections of different groups of animals and treatments as indicated; V indicates vehicle (PBS) alone treatment. The number of mice in each group are, untreated BLT1$^{+/+}$K-ras^{LA1} (n=7); PBS treated BLT1$^{+/+}$K-ras^{LA1} (n=5); CS treated BLT1$^{+/+}$K-ras^{LA1} (n=10); untreated BLT1$^{-/-}$K-ras^{LA1} (n=7); CS treated BLT1$^{-/-}$K-ras^{LA1} (n=10). Error bars in **b** and **d** denote mean ± SEM.*P < 0.025, ***P < 0.0003, n.s is non-significant; Mann Whitney U-test.

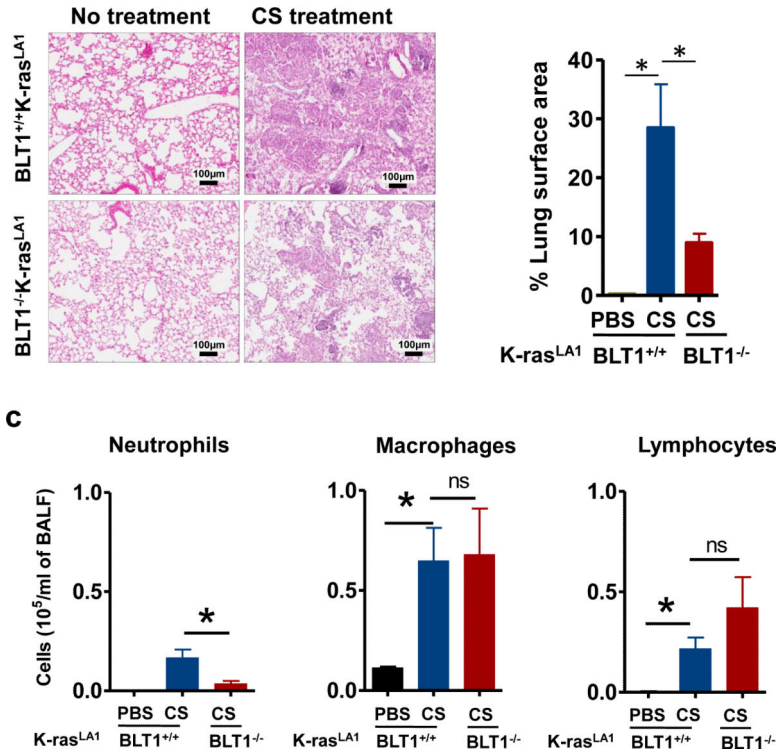

Figure 2. Absence of BLT1 attenuates lung inflammation in K-ras^{LA1} mice

Lungs from BLT1$^{+/+}$K-ras^{LA1} and BLT1$^{-/-}$K-ras^{LA1} mice exposed to CS for 60 days were assessed for inflammation and inflammatory cell recruitment. (**a**) Representative lung H&E sections show inflammation post CS treatment; scale bars, 100μm. (**b**) Lung inflammation was scored as the percentage of inflamed lung area to total lung area in H&E stained lung sections. The number of mice in each group are, PBS treated BLT1$^{+/+}$K-ras^{LA1} (n=3); CS treated BLT1$^{+/+}$K-ras^{LA1} (n=8); CS treated BLT1$^{-/-}$K-ras^{LA1} (n=10). (**c**) CS exposure induced recruitment of neutrophils, macrophages and lymphocytes into airways was assessed in whole lung lavage by flow cytometry as described in methods. The number of mice in each group are, PBS treated BLT1$^{+/+}$K-ras^{LA1} (n=3); CS treated BLT1$^{+/+}$K-ras^{LA1} (n=4); CS treated BLT1$^{-/-}$K-ras^{LA1} (n=5). Error bars in b, **c** denote mean ± SEM. *P < 0.04 Mann Whitney U-test.

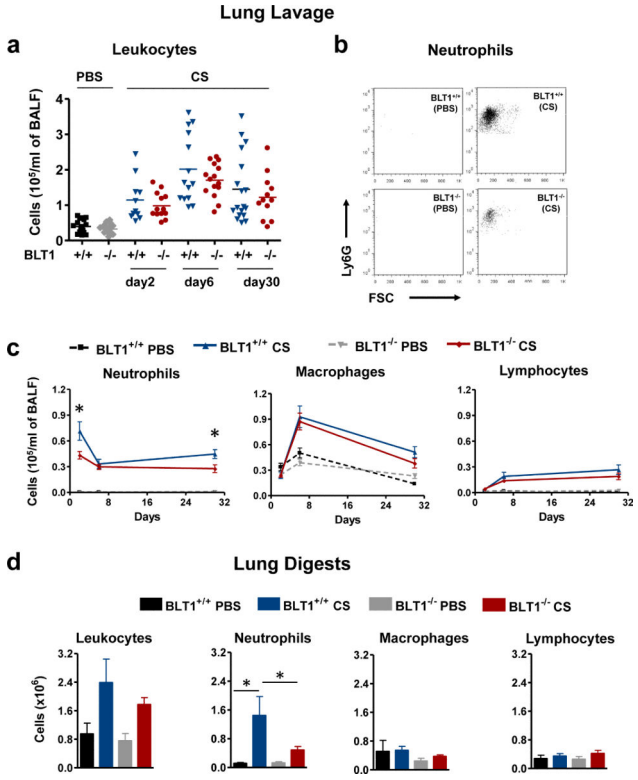

Figure 3. Attenuation of CS-induced lung neutrophil recruitment in the absence of BLT1

Eight weeks old BLT1$^{+/+}$ and BLT1$^{-/-}$ mice were exposed to CS. Inflammatory cell recruitment into airways (**a-c**) and lung interstitium (**d**) was assessed by flow cytometry using surface staining for cell specific markers. Analysis of whole lung lavage at indicated times show (**a**) number of total leukocytes; each dot represents a single mouse, (**b**) neutrophils 2 days post CS exposure in the flow-cytometry scatter plots and (**c**) number of neutrophils, macrophages and lymphocytes. Data represent at least 11 mice per group; difference between CS treated BLT1$^{+/+}$ and BLT1$^{-/-}$ group is indicated. (**d**) Analysis of unlavaged whole lung digests 2 days post CS exposure show number of total leukocytes, neutrophils, macrophages and lymphocytes. The number of mice in each group are, PBS treated BLT1$^{+/+}$ (n=3); CS treated BLT1$^{+/+}$ (n=5); PBS treated BLT1$^{-/-}$ (n=5); CS treated BLT1$^{-/-}$ (n=6). Error bars denote mean ± SEM. *P < 0.04 Mann Whitney U-test.

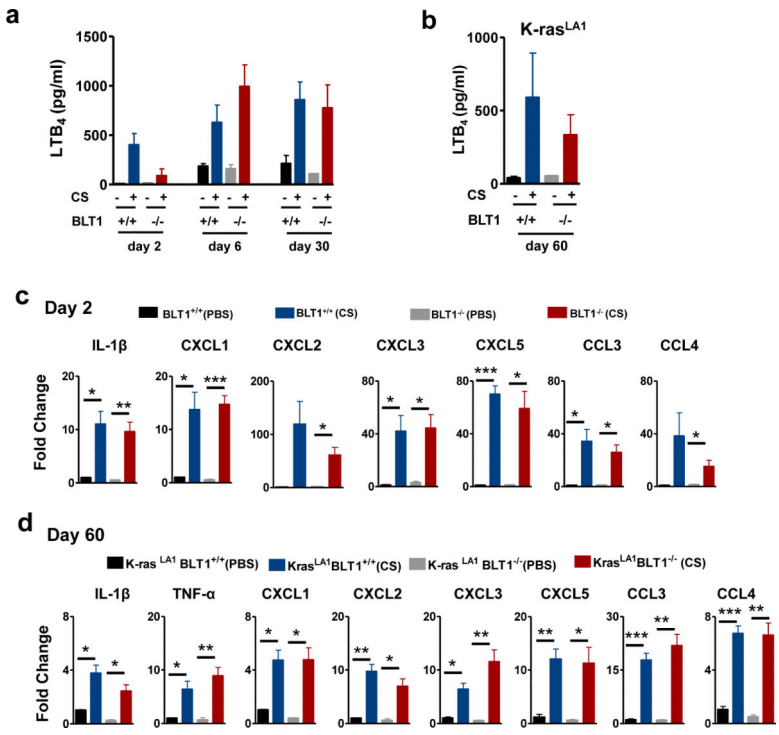

Figure 4. CS-induced neutrophil chemoattractants remain unaffected in the absence of BLT1

Mediators of CS-induced pulmonary inflammation were analyzed by accessing production of (**a**-**b**) LTB_4 in whole lung lavage fluids and (**c**-**d**) cytokines and chemokines in total lung RNA. LTB_4 levels in lung lavage fluids of (**a**) CS exposed BLT1$^{+/+}$ and BLT1$^{-/-}$ mice at indicated times and (**b**) of BLT1$^{+/+}$K-ras^{LA1} and BLT1$^{-/-}$K-ras^{LA1} mice exposed to CS for 60 days. Data are from at least 5 mice per group. Quantitative real-time PCR analysis of total lung RNA showing fold increase of neutrophil-active cytokines and chemokines in (**c**) BLT1$^{+/+}$ and BLT1$^{-/-}$ mice exposed to CS for 2 days and (**d**) BLT1$^{+/+}$K-ras^{LA1} and BLT1$^{-/-}$K-ras^{LA1} mice exposed to CS for 60 days. Fold change of mRNA levels over PBS treated BLT1$^{+/+}$ samples are shown; differences in mRNA levels are not significant between the CS exposed BLT1$^{+/+}$ and BLT1$^{-/-}$ groups. Data represent at least 5 mice per group; error bars denote mean ± SEM. *P < 0.03, **P < 0.009, ***P < 0.0007; Unpaired t-test.

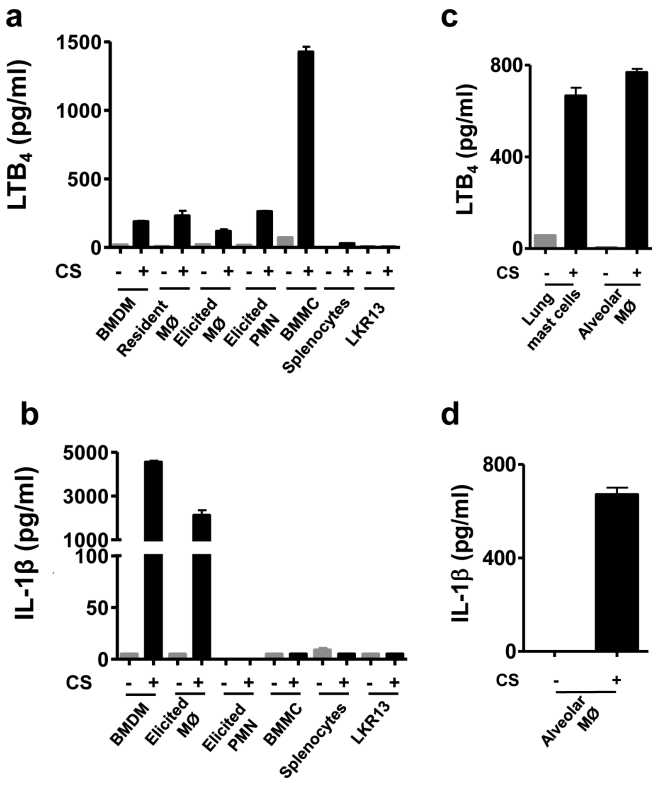

Figure 5. Cell type specificity of CS-induced LTB_4 and IL-1β production

Lung epithelial cell line (LKR13) and primary cells: macrophages, mast cells, neutrophils, splenocytes from wild-type (WT) were assessed for production of LTB_4 and IL-1β *in vitro* post CS stimulation. In triplicate cultures 0.3×10^6 of the indicated cell types were stimulated with 100μg/cm^2 of CS for six hours. **(a)** LTB_4 levels in culture supernatants of CS exposed ex-vivo cultured immune cells and lung epithelial cell line (LKR13) as indicated; MØ is macrophage, PMN is neutrophil, BMDM is bone-marrow derived macrophages, BMMC is bone-marrow derived mast cells. (**b**) IL-1β levels in the same culture supernatants as in panel **a**. The CS-induced LTB_4 (**c**) and IL-1β (**d**) production was determined in culture supernatants of alveolar macrophages and lung mast cells. Alveolar macrophages and lung mast cells were purified as described in methods and exposed to CS *in vitro*. Purity of the cell types were determined by flow cytometry. Thioglycollate elicited neutrophils and macrophages; resident peritoneal macrophages; lung mast cells were ≥ 95% pure, whereas BMMC, BMDM and alveolar macrophages were ≥ 99% pure. Error bars denote mean ± SEM. Data are representative of at least two independent experiments in triplicate cultures.

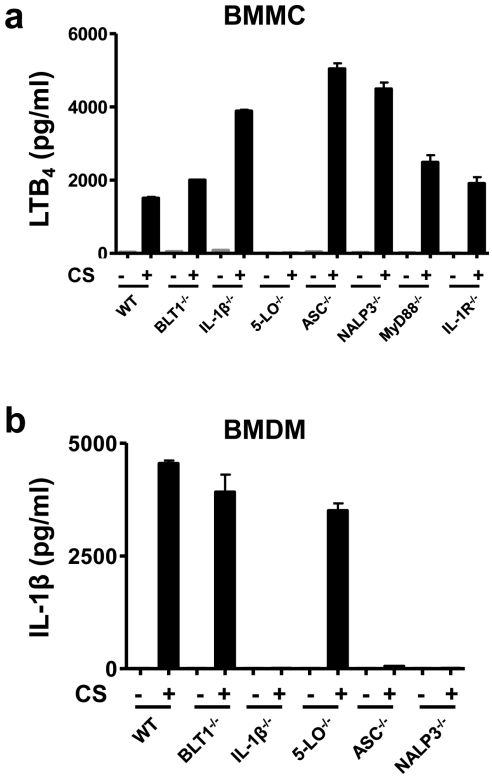

Figure 6. Independent regulation of LTB_4 and IL-1β production in CS exposed cells

Interdependence of CS-induced LTB_4 and IL-1β production was determined in cultured bone-marrow derived mast cells (BMMC) and bone-marrow derived macrophages (BMDM) from different gene knockout mice as indicated. In triplicate cultures 0.3×10^6 of (**a**) BMMCs or (**b**) BMDMs were stimulated with $100\mu g/cm^2$ of CS for six hours and (**a**) LTB_4 and (**b**) IL-1β levels were determined by EIA or ELISA, respectively. Purity of the cells was determined by flow cytometry. All cell types of indicated genotypes were ≥ 99% pure. Error bars denote mean ± SEM. Data are representative of at least two independent experiments performed in triplicate cultures.

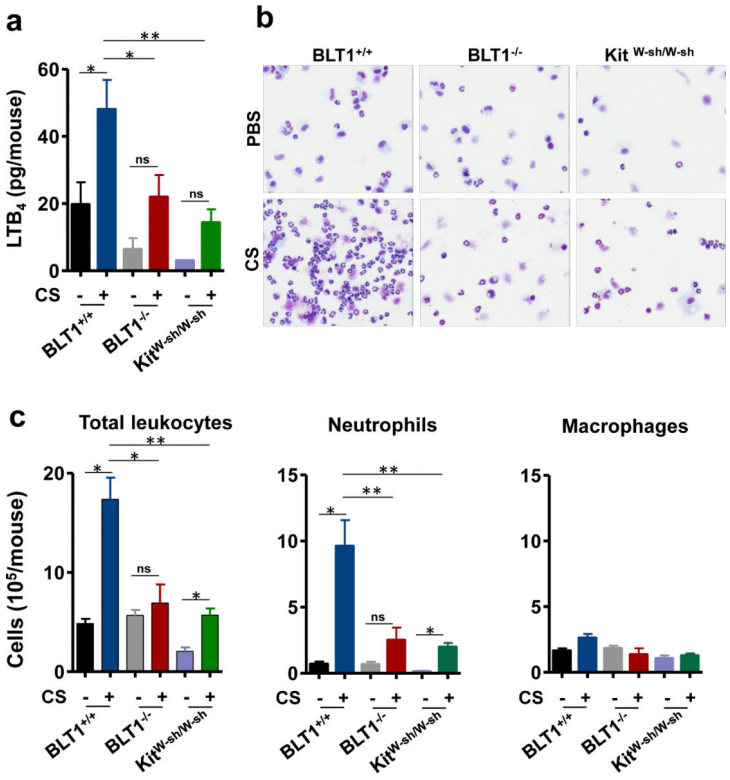

Figure 7. CS-induced neutrophil recruitment into the air pouch is dependent on LTB_4/BLT1 axis

CS induced inflammation in an air pouch was analyzed. Six hours post CS particle exposure the air pouch was lavaged with 3ml of buffer to assess LTB_4 levels and infiltrating immune cells. (**a**) LTB_4 levels, (**b**) leukocytes on cytospin slides and (**c**) total leukocytes, neutrophils and macrophages as identified by flow cytometry of the air pouch lavage fluid from mice of the indicated genotypes. Data are representative of at least five mice per group. Error bars denote mean ± SEM. *P < 0.02, **P <0.009; Mann Whitney U-test.

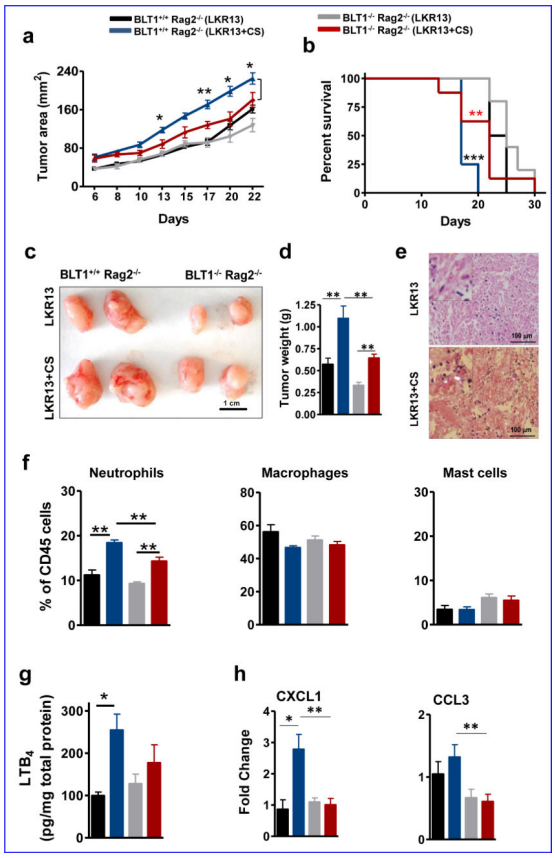

Figure 8. Absence of BLT1 protects from CS- promoted growth of implanted lung tumors

LKR13 cells along with CS particles were implanted subcutaneously into BLT1$^{+/+}$Rag2$^{-/-}$ or BLT1$^{-/-}$Rag2$^{-/-}$ mice and the kinetics of tumor growth, survival of mice and tumor inflammatory microenvironment was analyzed. (**a**) Tumor size in mice of indicated genotype and treatment are shown. The number of mice in each group are, LKR13 injected BLT1$^{+/+}$Rag2$^{-/-}$ (n=12); LKR13 with CS injected BLT1$^{+/+}$Rag2$^{-/-}$(n=10); LKR13 injected BLT1$^{-/-}$Rag2$^{-/-}$ (n=6); LKR13 with CS injected BLT1$^{-/-}$Rag2$^{-/-}$(n=7). (**b**) Kaplan-Meier survival curves of tumor bearing mice are shown. Data represent 8 mice per group; *** (black) indicates comparison between LKR13 and LKR13 with CS injected BLT1$^{+/+}$Rag2$^{-/-}$ groups; ** (red) indicates comparison between LKR13 with CS injected BLT1$^{+/+}$Rag2$^{-/-}$ and BLT1$^{-/-}$Rag2$^{-/-}$ groups. (**c**) Representative images of tumors sixteen days post implantation for the indicated genotype and treatment are shown; scale bars, 1cm. (**d**) Tumor weights at day 16 of LKR13 injected BLT1$^{+/+}$Rag2$^{-/-}$ (n=4); LKR13 with CS injected BLT1$^{+/+}$Rag2$^{-/-}$(n=6); LKR13 injected BLT1$^{-/-}$Rag2$^{-/-}$ (n=5); LKR13 with CS injected BLT1$^{-/-}$Rag2$^{-/-}$(n=7). (**e**) Deposited CS particles in tumor sections viewed under polarized light; scale bars, 100 μm; insets show CS particles at higher magnification. (**f**) Neutrophils, macrophages and mast cells expressed as percent of total tumor infiltrating immune cells identified by flow cytometry are shown. (**g**) LTB_4 levels measured in tumor homogenates and (**h**) quantitative real-time PCR analysis of total tumor RNA showing fold increase of neutrophil-active chemokines; fold change over BLT1$^{+/+}$Rag2$^{-/-}$ injected with LKR13 cells is shown. In **f-h** the number of mice in each group are, LKR13 injected

$BLT1^{+/+}Rag2^{-/-}$ (n=4), LKR13 injected $BLT1^{-/-}Rag2^{-/-}$ (n=4), LKR13 with CS injected $BLT1^{+/+}Rag2^{-/-}$ (n=7) and LKR13 with CS injected $BLT1^{-/-}Rag2^{-/-}$ (n=7). Error bars denote mean ± SEM. *P < 0.02, **P <0.009, ***P < 0.0007; Mann Whitney U-test.

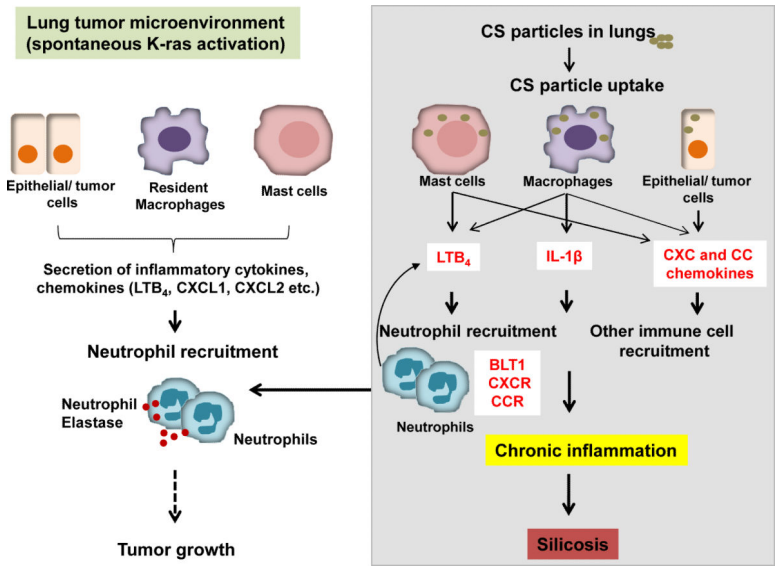

Figure 9. A schematic model for the role of LTB_4-BLT1 axis in CS accelerated lung tumor growth

Spontaneous activation of K-ras gene in the lungs induces an inflammatory microenvironment (intrinsic pathway) that promotes cancer-related inflammation and tumor growth. This study shows that exposure to crystalline silica particles induces chronic inflammation (extrinsic pathway) which likely accelerates lung tumor growth. LTB_4 produced by mast cells and IL1β, LTB_4, CXC/CC chemokines by macrophages and CXC/CC chemokines by lung epithelial cells in response to CS exposure leads to sustained neutrophil accumulation. LTB_4/BLT1 axis sets the pace of CS induced sterile inflammation thereby promoting lung tumor progression.